High adsorption capacity of Mg–Al-modified biochar for phosphate and its potential for phosphate interception in soil

Qin Zheng, Lanfang Yang, Dali Song, Shuai Zhang, Hang Wu, Shutian Li, Xiubin Wang

PII: S0045-6535(20)31663-5

DOI: https://doi.org/10.1016/j.chemosphere.2020.127469

Reference: CHEM 127469

To appear in: *ECSN*

Received Date: 24 February 2020

Revised Date: 26 May 2020

Accepted Date: 16 June 2020

Please cite this article as: Zheng, Q., Yang, L., Song, D., Zhang, S., Wu, H., Li, S., Wang, X., High adsorption capacity of Mg–Al-modified biochar for phosphate and its potential for phosphate interception in soil, *Chemosphere* (2020), doi: https://doi.org/10.1016/j.chemosphere.2020.127469.

Credit author statement:

Qin Zheng: Conceptualization, Methodology, Data curation, Formal analysis, Writing original draft preparation.
Lanfang Yang: Conceptualization, Supervision.
Dali Song: Visualization, Investigation.
Hang Wu: Methodology, Software.
Shutian Li: Writing-review and editing.
Xiubin Wang: Funding acquisition, Project administration, Supervision, Writing original draft preparation, Writing - review and editing.

High adsorption capacity of Mg–Al-modified biochar for phosphate and its potential for phosphate interception in soil[1]

Qin Zheng [a, b], Lanfang Yang [b], Dali Song [a], Shuai Zhang [a], Hang Wu [a], Shutian Li [a, □], Xiubin Wang [a, □]

[a] Institute of Agricultural Resource and Regional Planning, Chinese Academy of Agricultural Sciences/Key Lab of Plant Nutrition and Nutrient Cycling, Ministry of Agriculture, Beijing 100081, China.

[b] Hubei University, Wuhan 430062, China.

□ Corresponding author:

Institute of Agricultural Resources and Regional Planning, Chinese Academy of Agricultural Sciences, No. 12, Zhongguancun South Street, Beijing, 100081, China.

Tel: +86 10 82109745; Fax: +86 10 82106225.

E-mail address: wangxiubin@caas.cn (X. Wang), lishutian@caas.cn (S. Li).

[1] Abbreviations: MABC, Mg–Al-modified biochar; MBC, Mg-modified biochar; ABC, Al-modified biochar; BC, biochar; PZC, point of zero charge; TP, total phosphorus; PP, paniculate phosphorus; SOP, soluble organic phosphorus; SRP, soluble reactive phosphorus.

GRAPHICAL ABSTRACT

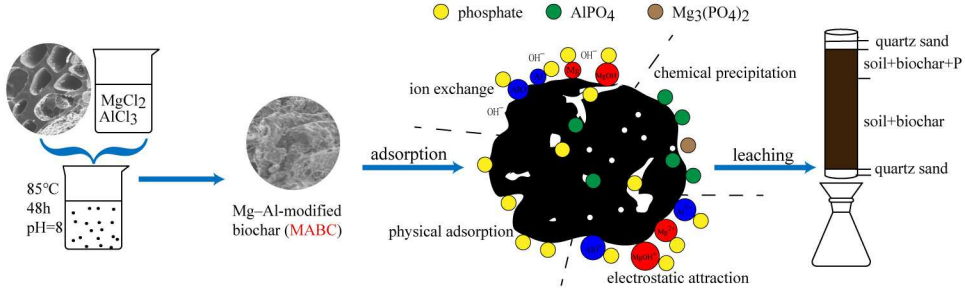

Abstract

In this study, Mg and/or Al modified biochars (MABC[1], MBC[2], ABC[3]) prepared by co-precipitation were to explore their phosphate adsorption capacity from aqueous solution and the potential for soil phosphate interception. The results revealed that MABC composites contained more functional groups than MBC and showed a higher surface area than ABC. The surface of MABC contained dispersed $MgAl_2O_4$, $Mg(OH)_2$, AlOOH and Al_2O_3 crystals that were associated with its enhanced maximum phosphate adsorption capacity (153.40 mg g^{-1}). According to Langmuir model, the maximum adsorption capacity of MABC was 15.91, 1.85, and 93.54 times the capacity of MBC, ABC, and raw biochar (BC[4]), respectively. The addition of MABC in red soil could significantly slow down the release of soil phosphorus, and MABC also had a stronger phosphate interception capacity (59.89%) than other BCs. In summary, MABC exhibits superior phosphate adsorption and interception capacity, making it ideal for treatment and prevention of phosphorus-polluted water.

Key words: Mg/Al; modified biochar; phosphate; adsorption; interception

[1] MABC: Mg–Al-modified biochar

[2] MBC: Mg-modified biochar

[3] ABC: Al-modified biochar

[4] BC: biochar

1. Introduction

Eutrophication is a water pollution phenomenon caused by excessive the cumulation of nitrogen, phosphorus, and other nutrients (Deng et al., 2019; Jonathan et al., 2010; Shi et al., 2020). Phosphorus is the main limiting factor for water eutrophication in the world (Li et al., 2020). Phosphorus enrichment poses an increasingly serious threat to ecosystem health and human survival globally (Meinikmann et al., 2015; Wang et al., 2020). Therefore, the removal of phosphorus is of great significance as a means of controlling water eutrophication and promoting environmental health.

Biochar as an adsorbent that can be used to remove phosphate from water, as has been shown in several recent studies (Gao et al., 2019; Zheng et al., 2019). However, biochar preparation prepared via traditional pyrolysis exhibit limited effective functional groups, specific surface area values, and anion exchange capacities (Wan et al., 2017; Zhu et al., 2020). Previous studies have also confirmed that raw biochar has a phosphate adsorption capacity of < 5 mg g^{-1} (Jung et al., 2017; Liao et al., 2018; Yu et al., 2016). In order to enhance the phosphate adsorption capacity of biochar, modifications are often used to activate biochar surface properties and structures (Gong et al., 2017; Novais et al., 2018a). Chen et al. (2018) confirmed that the relative content of C−H and −COOH increased by 3.55% and 8.48% in Mg-impregnated biochar, respectively, relative to raw biochar. Zhang and Gao et al. (2013) found that the surface of Al-modified biochar produced via pyrolysis contained

nanometer AlOOH crystals and had a large specific surface area. However, Fe-modified biochar prepared via direct hydrolysis exhibited decreased specific surface area (Micháleková-Richveisová et al., 2017). These different modification methods and metals have different effects on the surface structure and chemical properties of the resultant biochar (Gong et al., 2017; Novais et al., 2018b; Yin et al., 2018a). A number of studies have found that biochar modified using individual metals such as Zn, Ca and Bi exhibited better performance than did unmodified biochar in the context of phosphate adsorption (Jung and Ahn et al., 2016; Liu et al., 2019; Zhu et al., 2016), although the phosphate adsorption capacity of some modified biochar preparations remained low (Micháleková-Richveisová et al., 2017; Liao et al., 2018). As such, recent studies have focused on the development of bimetal modified biochar in order to achieve better adsorption capacity. Li et al. (2016) successfully developed Mg/Al-modified biochar using different Mg: Al ratios, and ultimately achieved an adsorption capacity of > 53.39 mg P g^{-1}. Yang et al. (2019) focused on different methods of using pyrolysis to prepare Mg/Al-LDHs as a phosphate adsorbent. However, few studies have explored whether biochar that has been single-metal or bimetal-modified via co-precipitation exhibits a better capacity to adsorb phosphate from water.

In addition, as a soil supplement biochar exhibits a profound pore structure and a strong adsorption capacity, having potential to improve soil structure, reduce nutrient leaching, and facilitate water and fertilizer preservation (Shi et al., 2020; Song et al., 2019). Chen et al. (2018) found that Mg-modified biochar decreased the phosphorus

leaching from sandy soil by 89.25%. Fe-modified biochar also prevented phosphorus loss by 86.40% (Wu et al., 2020). In contrast, a soil column leaching test performed by Riddle et al. (2018) revealed that there were no significant differences in this phosphorus retention effect when comparing magnetite-coated biochar to a no biochar treatment condition. These contradictory results are primarily due to differences in soil, type and dosage of modified biochar. While most studies have evaluated the effect of biochar or modified biochar on total phosphorus and available phosphorus leaching from saline and sandy soil (Wu et al., 2020; Chen et al., 2018; Kumari et al., 2014), few studies have explored the phosphorus fractions in leachates, particularly in the context of leaching from red soil.

In this study, in an effort to define better strategies for addressing those issues, we prepared modified BC composites via the impregnation of wheat straw BC with Mg and Al (MABC), Mg (MBC), or Al (ABC) salts. We then analyzed the phosphate adsorption activity of these composite materials. The aims of this study were i) to analyze BC structural properties via elemental analysis, Brunauer-Emmett-Teller (BET)-surface area (SA) analysis, scanning electron microscopy (SEM)-energy dispersive spectrometer (EDS), Fourier transform infrared spectroscopy (FTIR), and X-ray diffraction spectroscopy (XRD); □) to assess how BC dosage, initial solution pH, and initial phosphate concentrations impact the phosphate adsorption process for these materials; □) to examine the mechanistic basis for phosphate adsorption by these modified BCs through the modeling of this adsorption process; □) to understand the effect of BCs on the interception of phosphorus in acid red soil. Together, the

results of this study will yield a theoretical basis for the development of BC-based approaches to alleviate the phosphate contamination.

2. Materials and methods

2.1. Modified biochar preparation

Wheat straw were taken from the wheat producing area of Hubei Province, China. Straw samples were cut until fragments were < 5 mm in size, after which they were heated from room temperature to 600°C (10 °C min^{-1}) in a microwave muffle furnace (SX2, Shanghai Rongfeng, Scientific Instrument Inc., Shanghai, China) under an N_2 atmosphere. Samples were held at this maximal temperature for 2 h, after which they were cooled to yield raw BC. BC samples were them impregnated using solutions containing 0.5 mol L^{-1} $MgCl_2$ + 0.5 mol L^{-1} $AlCl_3$, 0.5 mol L^{-1} $MgCl_2$, or 0.5 mol L^{-1} $AlCl_3$ at a solid-to-liquid ratio of 1:20 g mL^{-1} (Yin et al., 2018b). For each of these preparations, 1.0 mol L^{-1} NaOH was used to adjust the solution to pH 8.0. Samples were then incubated at 85 ℃ for 48 h, followed by filtration, washing with deionized water (DW), and dried at 105 ℃. These resultant MABC, MBC, and ABC composites were then further cut to a particle size of < 2 mm prior to downstream utilization. Chemical reagents described above were from Weilaibo Biotechnology Co., Ltd (Beijing, China).

2.2. Batch experiments

Static adsorption experiments were used to assess the phosphate adsorption abilities of composite BC materials in aqueous solutions. Optimal adsorption conditions were sought across a range of BC dosages, initial pH values, and baseline phosphate concentrations. Under these optimal conditions, adsorption kinetics and isothermal adsorption models for these BC composite materials were established.

PO_4^{3-} adsorption as a function of the concentrations of modified BC preparations were assessed first. 0.05, 0.15, 0.25, 0.35, or 0.45 g of BCs were added to a 50 mL KH_2PO_4 solution (100 mg L^{-1}; pH 6.0). After shaking for 24 h at 180 rpm at room temperature, this mixture was filtered through a 0.45 μm aqueous filter, and phosphate concentrations within the filtrate were measured. The phosphate adsorption capacity is formulated as follows:

$$q_e = (C_0 - C_e)V/m, \quad (1)$$

where C_0 (mg g^{-1}) and C_e (mg g^{-1}) are the initial and equilibrium phosphate concentrations, respectively; m (g) is the mass of the adsorbent; and V (L) is the volume of the phosphate solution.

The different initial pH values of solution were adjusted to range from 3.0-10.0 by 1 mol L^{-1} HCl or 1 mol L^{-1} NaOH. Initial BC and phosphate concentrations for this experiment were 7 g L^{-1} and 100 mg L^{-1}, respectively. Following mixture preparation, samples were incubated for 24 h with shaking (180 rpm) and analyzed as above.

Lastly, the impact of baseline phosphate concentrations on BCs adsorption capacity by preparing a solution containing 7 g L^{-1} BCs and 10, 50, 100, 200, or 400 mg L^{-1} phosphate (pH 6.0) were assessed. Following mixture preparation, samples were incubated for 24 h with shaking (180 rpm) and analyzed as above.

BC phosphate adsorption kinetics were determined via combining a 50 mL solution (pH 6.0; 100 mg L^{-1} phosphate) containing 0.35 g BC. The supernatant was

collected and analyzed at different time intervals (0.08, 0.17, 0.25, 0.33, 0.5, 1, 1.5, 2.5, 4, 6, 8, 12, 24 h). BC phosphate adsorption capacity was calculated using Eqs. (2) and (3):

Pseudo − first − order $Q_t = q_e(1 - e^{-k_1 t})$, (2)

Pseudo − second − order $Q_t = k_2 q_e^2 t/(1 + k_2 q_e t)$, (3)

Where q_e and q_t (mg g^{-1}) correspond to phosphate concentrations at equilibrium time and at time t, respectively; k_1 (h^{-1}) and k_2 ($g \cdot mg^{-1} \cdot h^{-1}$) correspond to model-specific rate constants.

BC phosphate adsorption isotherms were performed by combining a 50 mL solution containing 0.35 g BC with a series of phosphate solutions (pH 6.0; 10- 2000 mg L^{-1} phosphate). These samples were shaken overnight, filtered, and phosphate concentrations were analyzed as above. The Langmuir and Freundlich isotherm models used for phosphate adsorption isotherms, were represented in Eqs. (4) and (5), respectively.

Langmuir isotherm model $Q_e = K_L Q C_e/(1 + k_L C_e)$, (4)

Freundlich isotherm model $Q_e = K_f C_e{}^{1/n}$, (5)

Where K_L (L mg^{-1}) and K_f ($mg^{(1-n)} \cdot L^n \cdot g^{-1}$)are the Langmuir and Freundlich constants, respectively; Q denotes the Langmuir maximum adsorption capacity (mg g^{-1}); C_e represents the equilibrium solution concentration (mg L^{-1}) of the phosphate; and n is the Freundlich linearity constant.

2.3. Leaching experiments

Samples of acid red soils (0 to 20 cm soil layer) were obtained from Chibi City,

Hubei Province, China (29°34′N, 113°55′E). The soil samples were naturally air-dried for one week in the room temperature, and filtered through a 2 mm sieve. The basic soil physicochemical characteristics were pH 4.72, total phosphorus (TP) 0.78 g kg^{-1}, available phosphorus (AP) 34.71 mg kg^{-1}.

A leaching experiment was conducted over 21 days to explore its potential for phosphate interception in soil. The five treatments including control (CK), MABC, MBC, ABC and BC were arranged with three replicates. Initially, Samples of MABC, MBC, ABC and BC were added separately at 1% by weight to soil and mixed thoroughly (Zhu et al., 2020). The mixtures of soil and biochar samples were divided into two parts (300g and 100g) and then packed into an acrylic tube with an inner diameter of 5 cm, a height of 25 cm, and small holes at the bottom. Before filling, a 100-mesh nylon membrane was stayed at the bottom of the column, and then 2 cm thick acid-washed quartz sand was added to distribute the water flow. 300 g of mixed soil sample was then added as lower layer soil. 0.075 g of KH_2PO_4 per column was evenly mixed into the upper mixed soil (100 g), and finally covered by another 2 cm thick quartz sand. DW was added to the soil column to saturation and the saturated soil column was incubated for 2 days before leaching.

The soil column was leached with DW on 3, 6, 9, 12, 15, 18, and 21 days following KH_2PO_4 application, with 220 mL of DW being added each time. All collected leachates were stored in an icebox in the dark at 4 °C prior to analyze the TP, particulate phosphorus (PP), soluble organic phosphorus (SOP) and soluble reactive phosphorus (SRP).

2.4. Analytical method

Total C, H, O, and N contents in BC preparations were assessed using an elemental analyzer (Vario EL □, Germany), whereas inductively coupled plasma-atomic emission spectrometry (Agilent 7700x, USA) was used to assess P, Mg and Al contents in these samples. BET surface area (S_{BET}) of samples was measured by N_2 adsorption at 77 K using Micromeritics ASAP 2020 (USA). A field emission gun SEM (Hitachi S4800, Japan) equipped with an EDS was used to assess BC morphology, while the surface functional group properties and crystalline phases of these BC preparations were assessed via FTIR spectrometry (Gangdong, FTIR-650, China) and XRD analysis (Rigaku D/max, Japan), respectively. Point of zero charge (PZC) value detection was conducted as previously described by Yin et al. (2018b). Chromogenic method was used to assess phosphate concentrations in solutions at an 880 nm wavelength by an ultraviolet-visible spectrophotometer (Daojin, UV2700, Japan). The concentration of TP in leachate were determined by above method after potassium persulfate digestion. The leachate samples were immediately filtered through a 0.45 μm filter membrane, and the filtrate was used for the determination of SRP. The filtrate was digested by potassium persulfate, and then the total soluble phosphorus (TSP) was measured the same as TP. The concentration of PP was determined by the difference value between TP and TSP, and the value of TSP minus SRP yields the concentration of SOP.

2.5. Statistical analysis

Measurement data are expressed as the mean of triplicate samples. All data were processed using Excel 2019 software. Statistical analysis was performed using software SPSS 23.0 and Origin 2018. Differences between treatments were examined by one-way ANOVA, and its significance was defined at $P< 0.05$.

3. Results and discussion

3.1. Modified biochar characterization

We found that the modification process significantly affected BC yield, surface structures, and physicochemical properties (Table 1). Following modification, the yields for all BC composites increased relative to raw BC as did the H and P content therein, while C and N contents decreased, consistent with previous results that were due to the removal of inorganic C during the biochar modification process (Zhou et al., 2017; Micháleková-Richveisová et al., 2017). As expected, MBC, ABC, and MABC samples exhibited significantly increased levels of Mg, Al, and Mg + Al, respectively, with EDS and XRD confirming these elements to be present in the form of oxides and hydroxides within the modified BC composites. The increased abundance of oxygen-containing functional groups within these modified BC structures was evidenced by relative increases in the O/C, H/C, and (O+N)/C ratios in these samples, suggesting that the modification process benefitted both the richness and diversity of functional groups. This was further confirmed based upon the strong adsorption peaks on the FTIR spectra of these modified BC samples (Wang et al., 2016). The S_{BET} of BC was 227.12 m^2 g^{-1}, which was higher than that of other BC samples derived from alternative crop waste, wood, animal droppings, or sludge under the same pyrolysis conditions (Hollister et al., 2013; Hong et al., 2019; Liu et al., 2020; Wang et al.,

232 2015). This was likely due to the higher lignin and cellulose contents in the straw used
233 for BC production in the present study (Novak et al., 2009). In this study, the S_{BET} of
234 MABC and MBC composites increased by 18.22% and 28.66%, respectively,
235 compared with BC. This may be due to the uniform of crystals of Mg compounds,
236 resulting in a rougher surface (Liao et al., 2018). The release of water vapor or other
237 compounds during biochar modification also can improve the structure of porosity,
238 which resulted in increased specific surface area (Yin et al., 2018b). This study also
239 found that the S_{BET} of biochar after being modified by Al was smaller than that of BC,
240 which was in line with the results of Michálеková-Richveisová et al. (2017). This may
241 be due to smaller size of AlOOH and Al_2O_3 formed on the surface of ABC, which could
242 more readily enter into the pores, causing blockage and decreased of S_{BET}. After
243 modification, the PZC of MABC, MBC and ABC were 7.6, 8.3 and 6.9, which
244 significantly increased than that of raw BC. This result indicated that modification
245 expanded the pH range of adsorption in the presence of electrostatic attraction.
246 SEM analyses were next used to assess the changes in BC pore structure that
247 occurred following the modification process. Whereas raw BC samples contained sharp
248 edges and corners, the modified BC composites contained surfaces that were
249 homogeneously covered with metal compounds (Fig. S1). There were stacked,
250 needle-like and flake-like compounds on the surfaces of MABC, MBC and ABC,
251 respectively. An analysis of the EDS spectrum revealed extremely high C and O peaks
252 in BC, whereas the MBC, ABC, and MABC composites exhibited additional peaks
253 corresponding to Mg, Al, and Mg + Al, respectively. The MBC EDS spectrum
254 confirmed that the surface acicular compounds on this composite were composed of

Mg (65.75%) and O (11.0%), which are the basic elements of MgO and $Mg(OH)_2$ (Liu et al., 2019), whereas the smooth ABC surface may be a consequence of AlOOH, $Al(OH)_3$, and Al_2O_3 formation. The MABC surface may contain all of these metal oxides and hydroxyl compounds, resulting in a more complex surface (Jung et al., 2015b).

The FTIR spectra of these BC composites were also analyzed (Fig. S2a). In these spectra, peaks at frequencies of 3400-3500 cm^{-1} and ~1597 cm^{-1} corresponded to –OH stretching vibrations of hydrogen-bonded groups and water molecules, while peaks at ~1410 cm^{-1} were attributable to $–CH_2–$ stretching aliphatic functional groups, and peaks at ~1128 cm^{-1} were attributable to O–C–O stretching vibrations (Li et al., 2017; Yin et al., 2018a). These functional groups were evident in both the modified and unmodified BC samples. In addition, the modified BC composites exhibited peaks at approximately 624 and 868 cm^{-1} that were assigned to the Mg–O or Al–O bonds (Jung et al., 2017; Yin et al., 2018b), consistent with the successful attachment of metal oxide or hydroxide compounds to the BC surface.

The XRD patterns of BC samples were showed in Fig. S3a. Raw BC samples exhibited absorption peaks at 2θ diffraction angles of 28.44°, 40.66°, 50.28°, 58.78° and 66.48° correspond to the crystal planes of (200), (220), (222), (400) and (420) of KCl (PDF No. 04-0587). ABC samples exhibited weak AlOOH and Al_2O_3 diffraction signals, suggesting that on the BC surface these compounds had a smaller particle size and lower crystallinity, indirectly confirming the presence of additional phosphate adsorption sites on these ABC composites. The MBC composite samples exhibited characteristic MgO peaks (PDF No. 43-1022) at 2θ diffraction peaks of 26.90° (111),

42.90° (200) and 62.28° (222). Although not detected in this analysis, $Mg(OH)_2$ may be present on MBC surfaces (Jung et al., 2015b). In addition to exhibiting surface crystals similar to those detected for ABC and MBC, MABC composites also contained $MgAl_2O_4$ crystals (PDF No. 73-1959) at 2θ angles of 31.26°, 36.88° and 44. 86°, which corresponded to the crystal planes (220), (311), and (420), respectively.

3.2. Phosphate adsorption

3.2.1. The effect of biochar dosage on phosphate adsorption

Previous studies have shown BC dosage to be one of the primary factors influencing its adsorption capacity (Cortes et al., 2019; Hairuddin et al., 2019). For all modified BC composites, we found that phosphate adsorption declined as BC dosage rose, whereas no such relationship was observed for raw BC (Fig. 1a). In contrast, these MABC, MBC, and ABC composite samples exhibited significantly enhanced phosphate removal rates, which were as high as 91.83% (7g L^{-1}), 22.33% (9 g L^{-1}), and 65.49% (9 g L^{-1}), respectively (Fig. 1b). These higher rates of phosphate removal were likely attributable to the increasing availability of effective functional groups and adsorbed active sites.

3.2.2. The effect of initial pH on phosphate adsorption

The initial pH of a solution can have a strong impact on both the phosphate ionization balance and the surface charge characteristics of adsorbent compounds found therein, resulting in marked changes in BC phosphate adsorption capacity (Ashekuzzaman and Jiang, 2014; Liu et al., 2019; Wan et al., 2017; Wang et al., 2018).

As pH values rose from 3.0 to 11.0, modified BC samples exhibited a phosphate adsorption capacity and removal rate that first rose and then fell, whereas raw BC exhibited a continuous reduction in adsorption capacity with rising pH (Fig. 1c and Fig. 1d). All modified BC composites exhibited optimal phosphate adsorption between a pH of 6.0 and 8.0, consistent with previous results from Jung et al. (2015b) and Hatami et al. (2018). HCl and NaOH were utilized to adjust the pH of these BC solutions, and the resultant presence of Cl^- and OH^- in these samples constrained BC-mediated phosphate adsorption at low and high pH, respectively (Ashekuzzaman and Jiang, 2014; Iftekhar et al., 2018). When the baseline pH of the sample solution was < 7.2, phosphate fractions were primarily present in the form of $H_2PO_4^-$, whereas the major form between pH 7.2 and 12.3 was HPO_4^{2-} (Wang et al., 2016). Previous studies demonstrated that BC samples were more readily able to adsorb $H_2PO_4^-$ than HPO_4^{2-}, as the former had a lower free energy of adsorption (Lǔ et al., 2013). When the baseline pH of the experimental solution was below PZC, the surface of these BC samples was positively charged, with electrostatic interactions being the primary driver of adsorption to the BC surface (Cui et al., 2011). The MABC, MBC, and ABC composites had PZC values of 7.6, 8.3, and 6.9, respectively (Table 1) , and the Al^{3+} ion coagulation process has been shown to be enhanced at a pH of 6.0 (Cheng et al., 2009). This, therefore, suggests that the optimal pH values for Mg- and Al-modified BC composites are different. As BC samples had a PZC value of < 3.0, electrostatic repulsion between the BC surface and phosphate ions was the predominant form of interaction between these compounds, explaining the observed decrease in phosphate adsorption capacity as the baseline pH of the experimental solution was increased.

3.2.3. The effect of initial phosphate concentration on phosphate adsorption

Across a baseline phosphate concentration range of 10-400mg/L, MBC samples exhibited concentration-dependent increases in phosphate adsorption capacity until reaching equilibrium (Fig. 1e). Amounts of phosphate adsorbed by MABC and ABC composites, in contrast, rose rapidly across this same concentration range. MABC removal rates initially increased and then decreased with increasing phosphate concentration (Fig. 1f), reaching a maximal removal rate at 100 mg L^{-1} (94.25%). MBC, ABC, and BC exhibited removal rates within the 14.03-26.62%, 53.81-61.01%, and 2.75-7.47% ranges, respectively. Qian et al. (2017) determined that phosphate adsorption was primarily driven via ligand exchange and electrostatic interactions, and the electrostatic interactions between MBC and phosphate were stronger than those between phosphate and MABC or ABC (Yao et al., 2013). This thus suggests that the excellent adsorption capacity of MABC maybe attributable to chemical exchange.

3.3. Biochar phosphate adsorption kinetics

Adsorption kinetic models can be used to deduce the main phosphate adsorption mechanisms of specific BC preparation (Gong et al., 2017). For the samples analyzed in the present study, three stages were evident during the phosphate adsorption process: a rapid stage of initial adsorption over the first 4 hours, during which time > 80% of adsorption capacity was reached; a stage if slow adsorption resulting from low phosphate concentrations in solution and the presence of fewer adsorption sites on BC surfaces (Liu et al., 2019), and an adsorption equilibrium stage (Fig. 2).

Pseudo-first-order models are commonly used to describe reversible adsorption

reactions that involve weak interactions between adsorbent and adsorbate, while pseudo-second-order models generally pertain to chemical reactions. Best-fit parameters for each of these models are shown in Table 2. The MABC and ABC adsorption data correlated best with a pseudo-second-order model (R^2 > 0.99), suggesting that phosphate adsorption occurs primarily via a chemical adsorption process (Jung and Ahn, 2016). For MBC and BC, we found that both pseudo-first-order and pseudo-second-order models fit very well with observed phosphate adsorption dynamics (R^2 > 0.99), suggesting that both physical and chemical adsorption restricted the adsorption rates for these BC composites.

3.4. Biochar phosphate adsorption isotherms

The isothermal adsorption fitting of the phosphate adsorption process for these different BC composites was conducted, with the fitting parameters being shown in Fig. 3 and Table 3. Sample adsorption data were more consistent with the Langmuir model than with the Freundlich model, indicating that BC-mediated phosphate adsorption was a monolayer and homogeneous process, with adsorption equilibrium being reached owing to the presence of insufficient adsorption sites to permit further adsorption (Novais et al., 2018a; Zhu et al., 2016). All modified BC composites tested in this study exhibited superior phosphate adsorption capacity relative to unmodified BC (MABC>ABC>MBC>BC). Using the Langmuir model, it was able to calculate a maximum theoretical phosphate adsorption capacity of 153.40 mg g^{-1} for MABC, with this value being 15.91, 1.85, and 93.54 times higher than that of MBC, ABC, and BC, respectively. The raw biochar exhibited a limited phosphate adsorption capacity (1.64

374 mg g^{-1}), which was consistent with other studies (Liao et al., 2018; Jung and Ahn et al.,
375 2016; Wang et al., 2016; Ashekuzzaman and Jiang., 2014). BC had well-developed
376 pore structure, a high pH and a net negatively charged surface, resulting in poor
377 phosphate affinity (Li et al., 2016). Zhu et al. (2019) postulated that the absence of
378 phosphate active sites would also limit the adsorption capacity of raw biochar. The
379 maximum adsorption capacity of MABC and ABC were higher than those of MBC and
380 BC, respectively. This may be related to the high surface AlOOH content of MABC and
381 ABC, which have been reported to exhibit an excellent phosphate adsorption capacity
382 (Zhang and Gao., 2013). Owing to their lager specific surface area and more abundant
383 functional groups (Cortes et al., 2019; Jung et al., 2015a), MABC and MBC exhibited
384 superior performance relative to ABC and BC, respectively. Yang et al. (2019) reported
385 that Mg/Al-LDH composites were associated with the highest phosphate adsorption
386 capacity (152.1 mg g^{-1}). Studies also revealed that Ca-Mg mixed biochar achieved
387 higher phosphate removal (95%) than did a single metal-modified biochar
388 (Ashekuzzaman and Jiang., 2014), while Yin et al. (2018b) confirmed that
389 Mg-modified biochar increased PO_4^{3-} adsorption capacity by two-fold relative to that
390 of Mg/Al-modified biochar. These different results may be due to differences in raw
391 materials and in the approaches to biochar modification used in these studies.
392 Phosphate adsorption data for Mg- or Al-modified BC samples are shown in Table 4. It
393 can be clearly seen that the adsorption capacity of Mg−Al-modified biochar for
394 phosphate was significantly higher than that of other BCs. In addition, the MABC
395 samples in this study had relatively simple preparation steps, with strong practicability.
396

3.5. Analysis of MABC phosphate adsorption mechanisms

The adsorption mechanisms of these different BC samples were better calefied via characterizing them following the completion of adsorption (Fig. S2b and Fig. S3b). Following adsorption, increases in phosphate group-associated bands at frequencies of 602, 794, 890 and 1381 cm^{-1} (Mangwandi et al., 2014; Yin et al., 2018a), were evident, whereas the previously detected −OH stretching vibration band at 3400-3500 cm^{-1} was almost completely absent on the surface of MABC, MBC, and MBC samples. This, therefore, suggested that −OH residues are involved in the phosphate adsorption process via doping into the BC materials or water (Liu et al., 2019). This FTIR spectral data also revealed that the main peak transmittance of MABC decreased and shifted after adsorption, indicating that phosphate can be adsorbed on the surface of biochar through ion exchange (Zhu et al., 2019).

After phosphate adsorption, the XRD pattern of MABC exhibited diffraction peaks could be identified as $AlPO_4$ (PDF No. 76-0226) and $Mg_3(PO_4)_2$ (PDF No. 35-0134). The result showed that phosphate was adsorbed by MABC through co-precipitation reaction. But there was no significant peak in the XRD patterns of BC and MBC, indicating that physical adsorption was the dominant mechanism for phosphate removal by them. This suggested that the following reactions may occur during the adsorption process:

$$AlOOH + PO_4^{3-} + 3H^+ \rightarrow AlPO_4 \downarrow + 2H_2O$$

$$AlOOH + HPO_4^{2-} + 2H^+ \rightarrow AlPO_4 \downarrow + 2H_2O$$

$$AlOOH + H_2PO_4^- + H^+ \rightarrow AlPO_4 \downarrow + 2H_2O$$

420 $Al^{3+} + PO_4^{3-} \rightarrow AlPO_4 \downarrow$

421 $3Mg^{2+} + 2PO_4^{3-} \rightarrow Mg_3(PO_4)_2 \downarrow$

422 At different initial solution pH values, the affinity of MABC for phosphate was
423 altered (Fig. 1c), revealing that the electrostatic forces between MABC and phosphate
424 were also involved in the adsorption process. Fig. 4 revealed the phosphate adsorption
425 mechanisms on the surface of MABC, which included electrostatic adsorption,
426 physical adsorption, ion exchange and chemical precipitation of phosphate.

427

428 *3.6. Effect of biochar on phosphorus leaching*

429

430 The experiment of column leaching was designed to investigate the BCs addition
431 effect on the phosphorus interception capacity in acidic red soil (Fig. 5a). The TP
432 content of modified BCs treatments increased first and then decreased over time,
433 while the treatment of raw BC kept decreasing. Phosphorus leaching in the context of
434 BC treatment was slightly higher than that observed following CK treatment at day 6,
435 which may be due to a loss of the phosphorus carried by the BC itself. Previous
436 studies have also found that BC application improved soil pH and AP content, thereby
437 promoting phosphorus leaching (Bai., 2013; Chen., 2018). In this study, maximal TP
438 content in CK, MABC, MBC, ABC, and BC treatment conditions was achieved on
439 days 3, 15, 9, 6 and 3, respectively, which may be attributable to the fact that modified
440 biochar can increase the residence time of soil phosphorus via adsorption, thereby
441 supplying phosphorus to soil for a longer period of time (Shi et al., 2020; Kameyama
442 et al., 2012). The cumulative amounts of phosphorus that leached from these four BC
443 treatments were lower than those from CK treatments (3.49 mg). These decreases were

significant and reached at 59.89%, 45.56%, 52.72% and 34.67% (P<0.05) for MABC, MBC, ABC, BC, respectively (Fig. 5b), indicating that BCs had an adsorption effect on soil phosphorus, and that modification promoted this adsorptive performance. This was similar to the study of Wu et al. (2020), but Mia et al. (2019) found that the addition of wood biochar increased soil organic matter (SOM) content and promoted phosphorus leaching. This may be because SOM competed with phosphorus for soil colloid adsorption sites and thereby reduced phosphorus fixation. In addition, due to the presence of other complex adsorption processes in soil environment, measured BC phosphate adsorption capacities in this soil column experiment were lower than those in batch experiments (Zhu et al., 2020). Relative to other treatments, the addition of MABC significantly decreased the amounts of SRP in the leachate (Fig. 5c), suggesting that phosphate compounds were adsorbed by MABC (Laird et al., 2010). SRP reductions were indicative of the decreasing bioavailability of phosphorus in leaching solution (Wen et al., 2020). The addition of MABC was able to reduce the threat of eutrophication to groundwater or lakes, and exhibited excellent environmental benefits.

After the leaching test, the TP content associated with different BC treatments increased significantly relative to control (Fig. 6a). This may be due to the addition of phosphorus carried by these BCs and due to their strong phosphate retention capacity. Relative to CK (42.61 mg kg^{-1}) treatment, the AP content in response to MABC (37.92 mg kg^{-1}) and ABC (40.46 mg kg^{-1}) treatment decreased slightly (Fig. 6b), and this was a consequence of co-precipitation between phosphate and metal oxides or hydroxides (Wu et al., 2020). The relative percentage of AP in thus upper layer under MABC, ABC, MBC, and BC treatment conditions were 39.85%, 26.78%, 31.16%, 27.96% (Fig. 6c), which were higher than those under CK treatment conditions

(13.91%), suggesting that the addition of BCs can prevent the movement of phosphates into lower soil layers.

4. Conclusion

The results of our analysis reveal that Mg−Al-modified biochar (MABC) exhibited superior phosphate adsorption and interception capacity, making it ideal for reducing the risk of water phosphorus enrichment. MABC possessed high surface area (268.51 m^2 g^{-1}), abundant oxygen-containing functional group (Mg−O and Al−O), and unique crystal ($MgAl_2O_4$). Compared with other BCs, MABC exhibited higher phosphate adsorption capacity of 153.40 mg g^{-1} at pH 6.0 and a dosage of 7 g L^{-1}, and stronger effect on reducing phosphorus leaching (59.89%) from the soil. Together these findings highlight a clear direction for future efforts to reuse straw resources in order to reduce water eutrophication.

Acknowledgements

This work was supported by the National Key Research and Development Program (2018YFD0200500) and the National Natural Science Foundation of China (No. 31372135). We also thank Dr. Mankouri and Dr. Bysouth for editing the English text of a draft of this manuscript.

References

493 Ashekuzzaman, S.M., Jiang, J.Q., 2014. Study on the sorption–desorption–regeneration
494 performance of Ca-, Mg- and CaMg-based layered double hydroxides for removing phosphate
495 from water. Chem. Eng. J. 246, 97-105.
496 Bai, Z., Li, H., Yang, X., Zhou, B., Shi, X., Wang, B., L, D., Shen, J., Chen, Q., Qin, W., Oenema, O.,
497 Zhang, F., 2013. The critical soil P levels for crop yield, soil fertility and environmental safety
498 in different soil types. Plant Soil. 372, 27-37.
499 Chen, Q., Qin, J., Cheng, Z., Huang, L., Sun, P., Chen, L., Shen, G., 2018. Synthesis of a stable
500 magnesium-impregnated biochar and its reduction of phosphorus leaching from soil.
501 Chemosphere. 199, 402-408.
502 Cheng, X., Huang, X., Wang, X., Zhao, B., Chen, A., Sun, D., 2009. Phosphate adsorption from
503 sewage sludge filtrate using zinc-aluminum layered double hydroxides. J. Hazard. Mater.
504 169(1-3), 958-964.
505 Cortes, L.N., Druzian, S.P., Streit, A.F.M., Sant'anna Cadaval Junior, T.R., Collazzo, G.C., Dotto,
506 G.L., 2019. Preparation of carbonaceous materials from pyrolysis of chicken bones and its
507 application for fuchsine adsorption. Environ. Sci. Pollut. R. 26(28), 28574-28583.
508 Cui, H.J., Wang, M.K., Fu, M.L., Ci, E., 2011. Enhancing phosphorus availability in
509 phosphorus-fertilized zones by reducing phosphate adsorbed on ferrihydrite using rice
510 straw-derived biochar. J. Soils Sediments. 11(7), 1135-1141.
511 Deng, R., Huang, D., Wan, J., Xue, W., Lei, L., Wen, X., Liu, X., Chen, S., Yang, Y., Li, Z., Li, B.,
512 2019. Chloro-phosphate impregnated biochar prepared by co-precipitation for the lead,
513 cadmium and copper synergic scavenging from aqueous solution. Bioresour. Technol. 293,
514 122102.

515 Gao, S., DeLuca, T.H., Cleveland, C.C., 2019. Biochar additions alter phosphorus and nitrogen
516 availability in agricultural ecosystems: A meta-analysis. Sci. Total Environ. 654, 463-472.
517 Gong, Y.P., Ni, Z.Y., Xiong, Z.Z., Cheng, L.H., Xu, X.H., 2017. Phosphate and ammonium
518 adsorption of the modified biochar based on Phragmites australis after phytoremediation.
519 Environ. Sci. Pollut. R. 24(9), 8326-8335.
520 Hairuddin, M.N., Mubarak, N.M., Khalid, M., Abdullah, E.C., Walvekar, R., Karri, R.R., 2019.
521 Magnetic palm kernel biochar potential route for phenol removal from wastewater. Environ.
522 Sci. Pollut. R. 26(34), 35183-35197.
523 Hatami, H., Fotovat, A., Halajnia, A., 2018. Comparison of adsorption and desorption of phosphate
524 on synthesized Zn-Al LDH by two methods in a simulated soil solution. Appl. Clay Sci. 152,
525 333-341.
526 Hollister, C.C., Bisogni, J.J., Lehmann, J., 2013. Ammonium, nitrate, and phosphate sorption to and
527 solute leaching from biochars prepared from Corn Stover (L.) and Oak Wood (spp.). J.
528 Environ. Qual. 42(1), 137-144.
529 Hong, Y., Xu, Z., Feng, C., Xu, D., Wu, F., 2019. The Preparation of Biochar Particles from Sludge
530 and Corncobs and Its Pb($^{2+}$) Adsorption Properties. Bull. Environ. Contam. Toxicol. 103(6),
531 848-853.
532 Iftekhar, S., Kucuk, M.E., Srivastava, V., Repo, E., Sillanpaa, M., 2018. Application of
533 zinc-aluminium layered double hydroxides for adsorptive removal of phosphate and sulfate:
534 Equilibrium, kinetic and thermodynamic. Chemosphere. 209, 470-479.
535 Jung, K.W., Ahn, K.H., 2016. Fabrication of porosity-enhanced MgO/biochar for removal of
536 phosphate from aqueous solution: Application of a novel combined electrochemical

modification method. Bioresour. Technol. 200, 1029-1032.

Jung, K.W., Hwang, M.J., Jeong, T.U., Ahn, K.H., 2015a. A novel approach for preparation of modified-biochar derived from marine macroalgae: Dual purpose electro-modification for improvement of surface area and metal impregnation. Bioresour. Technol. 191, 342-345.

Jung, K.W., Jeong, T.U., Hwang, M.J., Kim, K., Ahn, K.H., 2015b. Phosphate adsorption ability of biochar/Mg-Al assembled nanocomposites prepared by aluminum-electrode based electro-assisted modification method with $MgCl_2$ as electrolyte. Bioresour. Technol. 198, 603-610.

Jung, K.W., Lee, S., Lee, Y.J., 2017. Synthesis of novel magnesium ferrite ($MgFe_2O_4$)/biochar magnetic composites and its adsorption behavior for phosphate in aqueous solutions. Bioresour. Technol. 245(Pt A), 751-759.

Jonathan, M.A., Deniz, O¨zkundakci., David, P.H., 2010. Nitrogen and phosphorus limitation of phytoplankton growth in New Zealand lakes: implications for eutrophication control. Ecosystems. 13, 966-977.

Kameyama, K., Miyamoto, T., Shiono, T., Shinogi, Y., 2012. Influence of sugarcane bagasse-derived biochar application on nitrate leaching in calcaric dark red soil. J. Environ. Qual. 41(4), 1131-1137.

Kumari, K.G.I.D., Moldrup, P., Paradelo M., Elsgaard, L., Hauggaard-Nielsen, H., Jonge, L.W., 2014. Effects of biochar on air and water permeability and colloid and phosphorus leaching in soils from a natural calcium carbonate gradient. J. Environ. Qual. 43(2), 647-657.

Laird, D., Fleming, P., Wang, B., Horton, R., Karlen, D., 2010. Biochar impact on nutrient leaching from a Midwestern agricultural soil. Geoderma. 158(3-4), 436-442.

559 Li, R., Wang, J.J., Zhou, B., Awasthia, M.K., Alia, A., Zhang, Z., Gastonb, L.A., Lahoria, A.H.,
560 Mahara, A., 2016. Enhancing phosphate adsorption by Mg/Al layered double hydroxide
561 functionalized biochar with different Mg/Al ratios. Sci. Total Environ. 559, 121-129.
562 Li, R., Wang, J.J., Zhou, B., Zhang, Z., Liu, S., Lei, S., Xiao, R., 2017. Simultaneous capture
563 removal of phosphate, ammonium and organic substances by MgO impregnated biochar and
564 its potential use in swine wastewater treatment. J. Clean. Prod. 147, 96-107.
565 Li, S., Lin, Z., Liu, M., Jiang, F., Chen, J., Yang, X., Wang, S., 2020. Effect of ferric chloride on
566 phosphorus immobilization and speciation in Dianchi Lake sediments. Ecotox. Environ. Safe.
567 197, 110637.
568 Liao, T., Li, T., Su, X., Yu, X., Song, H., Zhu, Y., Zhang, Y., 2018. $La(OH)_3$-modified magnetic
569 pineapple biochar as novel adsorbents for efficient phosphate removal. Bioresour. Technol.
570 263, 207-213.
571 Liu, S., Pu, S., Deng, D., Huang, H., Yan, C., Ma, H., Razavi, B.S., 2020. Comparable effects of
572 manure and its biochar on reducing soil Cr bioavailability and narrowing the rhizosphere
573 extent of enzyme activities. Environ Int. 134, 105277.
574 Liu, X., Shen, F., Smith, R.L., Jr., Qi, X., 2019. Black liquor-derived calcium-activated biochar for
575 recovery of phosphate from aqueous solutions. Bioresour. Technol. 294, 122198.
576 Lǔ, J., Liu, H., Liu, R., Zhao, X., Sun, L., Qu, J., 2013. Adsorptive removal of phosphate by a
577 nanostructured Fe–Al–Mn trimetal oxide adsorbent. Powder Technology. 233, 146-154.
578 Mangwandi, C., Albadarin, A.B., Glocheux, Y., Walker, G.M., 2014. Removal of ortho-phosphate
579 from aqueous solution by adsorption onto dolomite. J. Environ. Chem. Eng. 2(2), 1123-1130.
580 Meinikmann, K., Hupfer, M., Lewandowski, J., 2015. Phosphorus in groundwater discharge-A

potential source for lake eutrophication. J. Hydrol. 524, 214-226.

Mia, S., Singh, B., Dijkstra, F.A., 2019. Chemically oxidized biochar increases ammonium-^{15}N recovery and phosphorus uptake in a grassland. Biol. Fertil. Soils. 55, 577-588.

Micháleková-Richveisová, B., Fristak, V., Pipiska, M., Duriska, L., Moreno-Jimenez, E., Soja, G., 2017. Iron-impregnated biochars as effective phosphate sorption materials. Environ. Sci. Pollut. R. 24(1), 463-475.

Novais, S.V., Zenero, M.D.O., Barreto, M.S.C., Montes, C.R., Cerri, C.E.P., 2018a. Phosphorus removal from eutrophic water using modified biochar. Sci. Total Environ. 633, 825-835.

Novais, S.V., Zenero, M.D.O., Tronto, J., Conz, R.F., Cerri, C.E.P., 2018b. Poultry manure and sugarcane straw biochars modified with $MgCl_2$ for phosphorus adsorption. J. Environ. Manage. 214, 36-44.

Novak, J.M., Busscher, W.J., Laird, D.L., Ahmedna, M., Watts, D.W., Niandou, M.A.S., 2009. Impact of Biochar Amendment on Fertility of a Southeastern Coastal Plain Soil. Soil Science. 174(2), 105-112.

Qian, J., Shen, M., Wang, P., Wang, C., Hu, J., Hou, J., Ao, Y., Zheng, H., Li, K., Liu, J., 2017. Co-adsorption of perfluorooctane sulfonate and phosphate on boehmite: Influence of temperature, phosphate initial concentration and pH. Ecotoxicol. Environ. Saf. 137, 71-77.

Shi, W., Ju, Y., Bian, R., Li, L., Joseph, S., Mitchell, D.R.G., Munroe, P., Taherymoosavi, S., Pan, G., 2020. Biochar bound urea boosts plant growth and reduces nitrogen leaching. Sci. Total Environ. 701, 134424.

Song, D.L., Xi, X.Y., Zheng, Q., Liang, G.Q., Zhou, W., Wang, X.B., 2019. Soil nutrient and microbial activity responses to two years after maize strawbiochar application in a calcareous

soil. Ecotox. Environ. Safe. 180, 348-356.

Wan, S., Wang, S., Li, Y., Gao, B., 2017. Functionalizing biochar with Mg-Al and Mg-Fe layered double hydroxides for removal of phosphate from aqueous solutions. J. Ind. Eng. Chem. 47, 246-253.

Wang, B., Lian, G., Lee, X., Gao, B., Li, L., Liu, T., Zhang, X., Zheng, Y., 2020. Phosphogypsum as a novel modifier for distillers grains biochar removal of phosphate from water. Chemosphere. 238, 124684.

Wang, S., Kong, L., Long, J., Su, M., Diao, Z., Chang, X., Chen, D., Song, G., Shih, K., 2018. Adsorption of phosphorus by calcium-flour biochar: Isotherm, kinetic and transformation studies. Chemosphere. 195, 666-672.

Wang, X., Zhou, W., Liang, G., Song, D., Zhang, X., 2015. Characteristics of maize biochar with different pyrolysis temperatures and its effects on organic carbon, nitrogen and enzymatic activities after addition to fluvo-aquic soil. Sci. Total Environ. 538, 137-144.

Wang, Z., Shen, D., Shen, F., Li, T., 2016. Phosphate adsorption on lanthanum loaded biochar. Chemosphere. 150, 1-7.

Wen, S., Wang, H., Wu, T., Yang, J., Jiang, X., Zhong, J., 2020. Vertical profiles of phosphorus fractions in the sediment in a chain of reservoirs in North China: Implications for pollution source, bioavailability, and eutrophication. Sci. Total Environ. 704, 135318.

Wu, L.P., Zhang, S.R., Wang, J., Ding, X.D., 2020. Phosphorus retention using iron (II/III) modified biochar in saline alkaline soils: Adsorption, column and field tests. Environ. Pollut. 261, 114223.

Yang, F., Zhang, S., Sun, Y., Tsang, D.C.W., Cheng, K., Ok, Y.S., 2019. Assembling biochar with

various layered double hydroxides for enhancement of phosphorus recovery. J. Hazard. Mater, 365, 665-673.

Yao, Y., Gao, B., Chen, J., Zhang, M., Inyang, M., Li, Y., Alva, A., Yang, L., 2013. Engineered carbon (biochar) prepared by direct pyrolysis of Mg-accumulated tomato tissues: characterization and phosphate removal potential. Bioresour. Technol. 138, 8-13.

Yin, Q., Ren, H., Wang, R., Zhao, Z., 2018a. Evaluation of nitrate and phosphate adsorption on Al-modified biochar: Influence of Al content. Sci. Total Environ. 631-632, 895-903.

Yin, Q., Wang, R., Zhao, Z., 2018b. Application of Mg–Al-modified biochar for simultaneous removal of ammonium, nitrate, and phosphate from eutrophic water. J. Clean. Prod. 176, 230-240.

Yu, P., Xue, Y., Gao, F., Liu, Z., Cheng, X., Yang, K., 2016. Phosphorus Removal from Aqueous Solution by Pre- or Post-Modified Biochars Derived from Agricultural Residues. Water Air Soil Pollut. 227(1), 370.

Zhang, M., Gao, B., 2013. Removal of arsenic, methylene blue, and phosphate by biochar/AlOOH nanocomposite. Chem. Eng. J. 226, 286-292.

Zheng, B.X., Ding, K., Yang, X.R., Wadaan, M.A.M., Hozzein, W.N., Penuelas, J., Zhu, Y.G., 2019. Straw biochar increases the abundance of inorganic phosphate solubilizing bacterial community for better rape (Brassica napus) growth and phosphate uptake. Sci. Total Environ. 647, 1113-1120.

Zhou, L., Huang, Y., Qiu, W., Sun, Z., Liu, Z., Song, Z., 2017. Adsorption properties of nano-MnO_2-biochar composites for copper in aqueous solution. Molecules. 22(1), 173.

Zhu, N., Yan, T., Qiao, J., Cao, H., 2016. Adsorption of arsenic, phosphorus and chromium by

647 bismuth impregnated biochar: Adsorption mechanism and depleted adsorbent utilization.
648 Chemosphere. 164, 32-40.
649 Zhu, S., Zhao, J., Zhao, N., Yang, X., Chen, C., Shang, J., 2020. Goethite modified biochar as a
650 multifunctional amendment for cationic Cd(II), anionic As(III), roxarsone, and phosphorus in
651 soil and water. J. Clean. Prod. 247, 119579.

Table 1

Elemental composition and physicochemical properties of different biochars.

Samples	Elemental composition (100%)							Atomic ratio			Yield (100%)	S_{BET} ($m^2 g^{-1}$)	PZC
	C	H	O	N	Mg	Al	P	O/C	H/C	(O+N)/C			
MABC	43.08	2.03	12.94	0.41	10.35	16.77	1.32	0.30	0.05	0.31	38.64	268.51	7.6
MBC	54.55	2.34	15.49	0.55	18.98	2.07	1.29	0.36	0.07	0.37	30.29	292.21	8.3
ABC	46.83	3.14	16.98	0.33	1.00	18.41	1.87	0.28	0.04	0.29	35.64	169.60	6.9
BC	79.67	1.98	13.77	1.15	1.68	1.77	1.15	0.17	0.02	0.19	25.35	227.12	2.1

Table 2

Parameters of phosphate adsorption kinetic on different biochars.

Samples	Pseudo first-order model			Pseudo second-order model		
	k_1 (h^{-1})	q_e (mg g^{-1})	R^2	k_2 (g mg^{-1} h^{-1})	q_e (mg g^{-1})	R^2
MABC	1.244	13.119	0.917	0.153	13.629	0.993
MBC	0.481	2.861	0.994	0.118	3.631	0.990
ABC	2.000	8.704	0.976	0.300	8.983	0.993
BC	0.685	1.456	0.998	0.535	1.577	0.991

Table 3

Parameters of phosphate adsorption isotherm on different biochars.

Samples	Langmuir models			Freundlich models		
	K_L ($L\ mg^{-1}$)	Q ($mg\ g^{-1}$)	R^2	n	K_f $[mg^{(1-n)}L^n g^{-1}]^{-1}$	R^2
MABC	0.0036	153.400	0.919	2.284	5.931	0.874
MBC	0.0076	9.639	0.932	3.413	1.072	0.753
ABC	0.0033	82.783	0.992	2.208	2.726	0.948
BC	0.0458	1.642	0.788	7.869	0.659	0.369

Table 4

Maximum phosphate adsorption capacity of different adsorbent.

Absorbents	Q_{max} (mg g^{-1})	Methods	Reference
$MgCl_2$ modified	17.6	Pre-modified	(Novais et al., 2018b)
Pseudo-boehmite (pseudo-γ-Al_2O_3)	13.6	-	(Yang et al., 2007)
Al-modified biochar (Al amount=20%)	57.49	Pre-modified	(Yin et al., 2018a)
Aluminum electrode	31.28	Electrical	(Jung et al., 2015a)
MgAl-LDH ultra-fine composites	410	Post-modified	(Zhang et al., 2013)
Mg modified biochar	9.639	Post-modified	This study
Al modified biochar	82.783	Post-modified	This study
Mg–Al modified biochar	153.400	Post-modified	This study

Figure captions:

Fig. 1. The phosphate adsorption rate and removal rate of all biochars on different dosage (a and b), initial solution pH (c and d), and initial phosphate concentration (e and f). Error bars represent the standard error of the mean (n= 3). Abbreviations: MABC, Mg–Al-modified biochar; MBC, Mg-modified biochar; ABC, Al-modified biochar; BC, biochar.

Fig. 2. Adsorption kinetics of phosphate on different biochars. Error bars represent standard error of the mean (n=3). Abbreviations: MABC, Mg–Al-modified biochar; MBC, Mg-modified biochar; ABC, Al-modified biochar; BC, biochar.

Fig. 3. Adsorption isotherms of phosphate on different biochars. Error bars represent standard error of the mean (n=3). Abbreviations: MABC, Mg–Al-modified biochar; MBC, Mg-modified biochar; ABC, Al-modified biochar; BC, biochar.

Fig. 4. The mechanisms of phosphate adsorption on MABC. Abbreviations: MABC, Mg–Al-modified biochar.

Fig. 5. (a) The dynamic amount of TP in leachates. (b) The cumulative amount of TP in leachates. (c) The proportion of different phosphorus forms. Error bars represent standard error of the mean (n=3) and lowercase letters indicate significant di□erence among the di□erent treatments (P< 0.05). Abbreviations: MABC, Mg–Al-modified biochar; MBC, Mg-modified biochar; ABC, Al-modified biochar; BC, biochar; TP,

total phosphorus; PP, paniculate phosphorus; SOP, soluble organic phosphorus; SRP, soluble reactive phosphorus.

Fig. 6. Soil TP (a) and AP (b) content after leaching experiment. (c) Relative percentage of AP in difference soil layers. Error bars represent standard error of the mean (n=3) and lowercase letters indicate significant di□erences among the di□erent treatments ($P < 0.05$). Abbreviations: MABC, Mg–Al-modified biochar; MBC, Mg-modified biochar; ABC, Al-modified biochar; BC, biochar; TP, total phosphorus; AP, available phosphorus.

Fig. 1

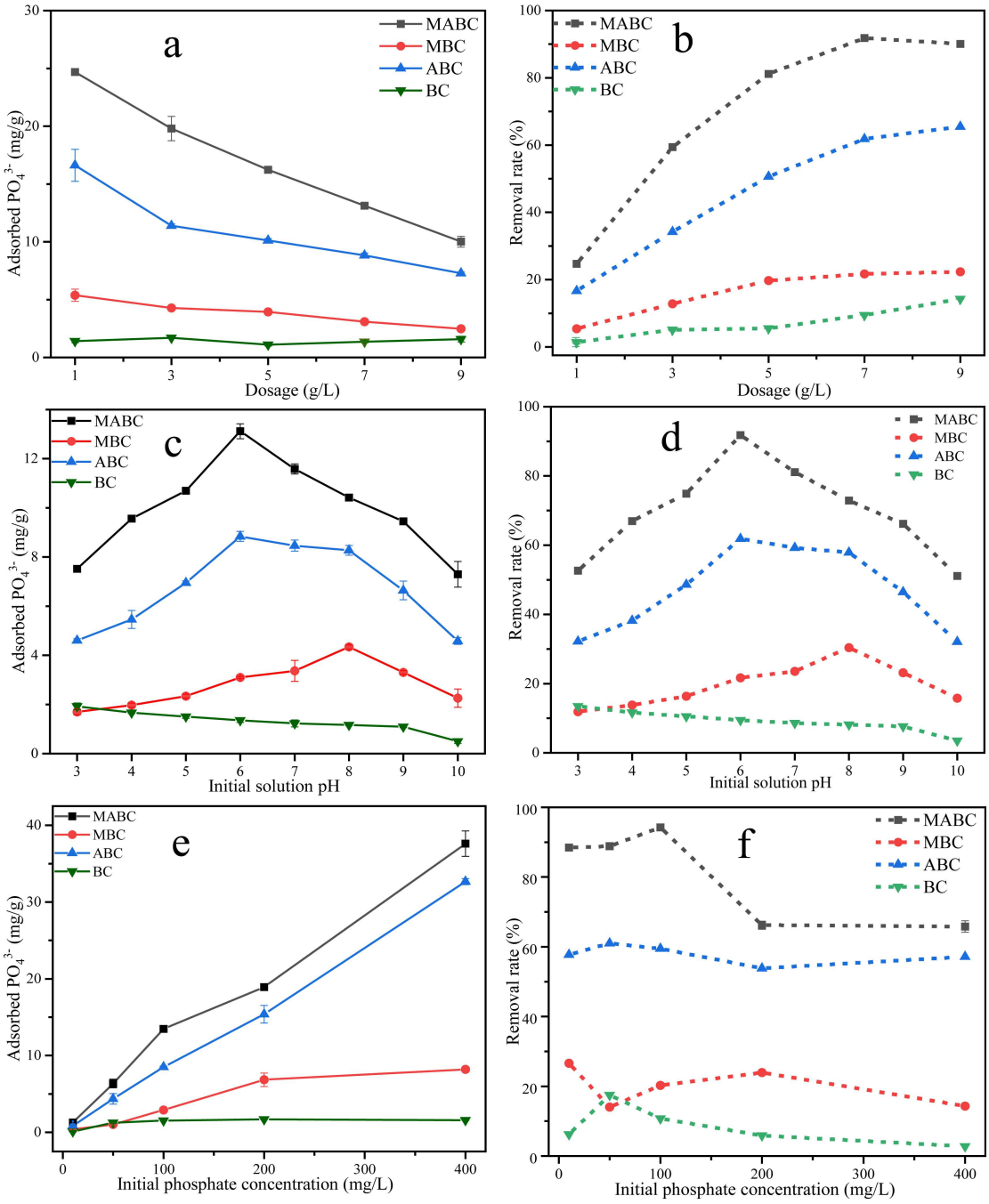
a
MABC
MBC
ABC
BC
Adsorbed PO_4^{3-} (mg/g)
Dosage (g/L)
b
Removal rate (%)
Dosage (g/L)
c
Adsorbed PO_4^{3-} (mg/g)
Initial solution pH
d
Removal rate (%)
Initial solution pH
e
Adsorbed PO_4^{3-} (mg/g)
Initial phosphate concentration (mg/L)
f
Removal rate (%)
Initial phosphate concentration (mg/L)

Fig. 2

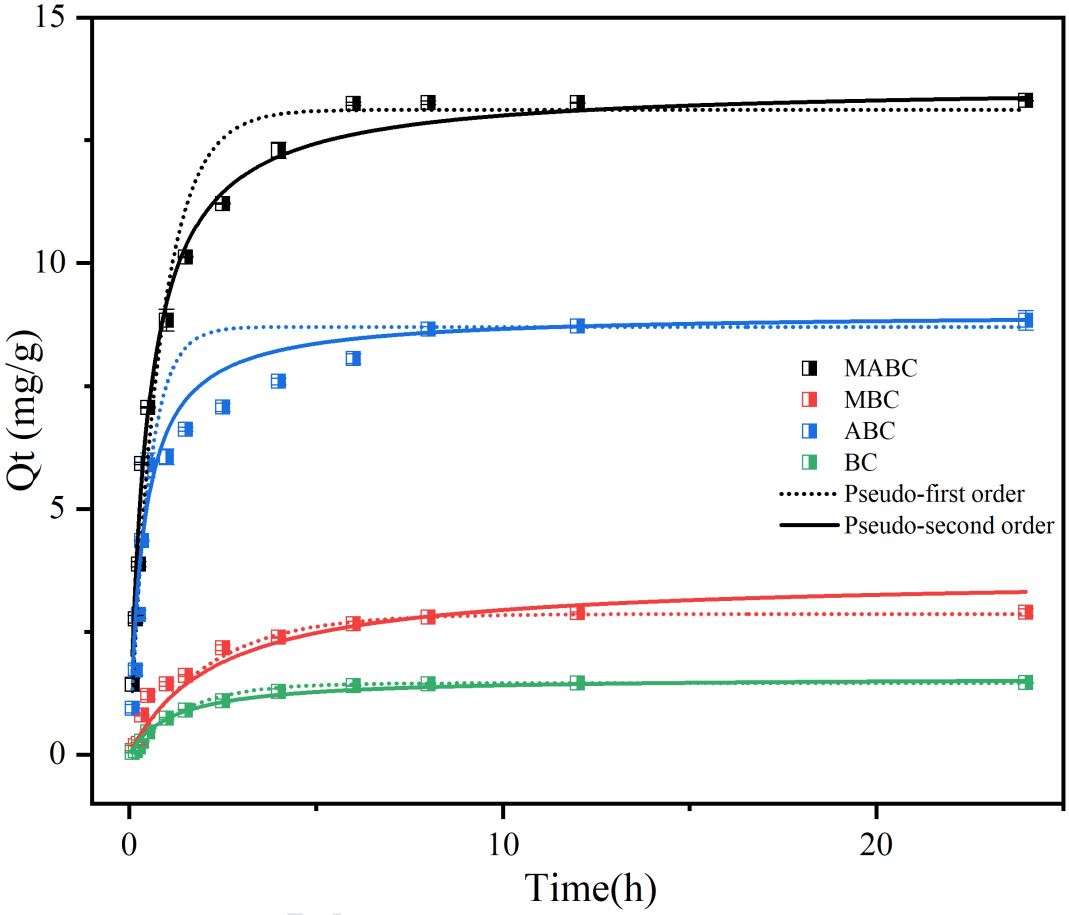
15
10
5
0
Qt (mg/g)
0
10
20
Time(h)
MABC
MBC
ABC
BC
Pseudo-first order
Pseudo-second order

Fig. 3

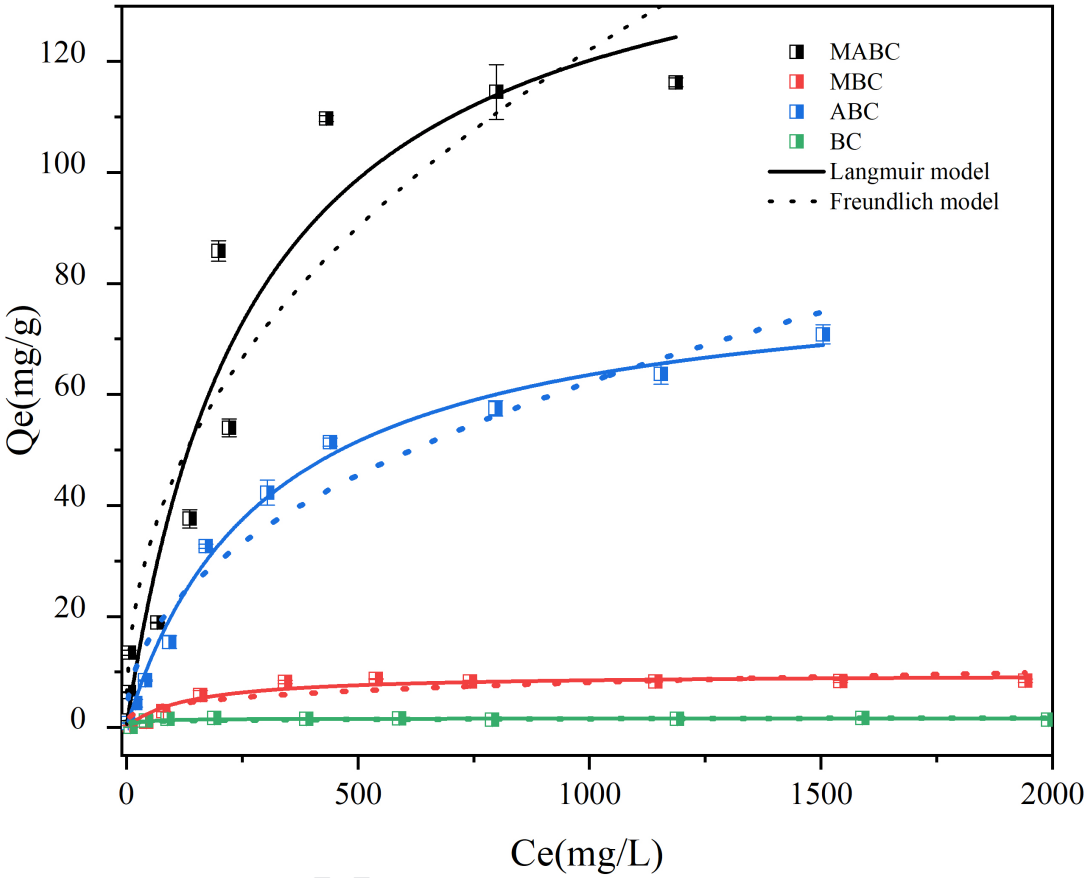
MABC
MBC
ABC
BC
Langmuir model
Freundlich model
Qe(mg/g)
Ce(mg/L)
0
20
40
60
80
100
120
0
500
1000
1500
2000

Fig. 4

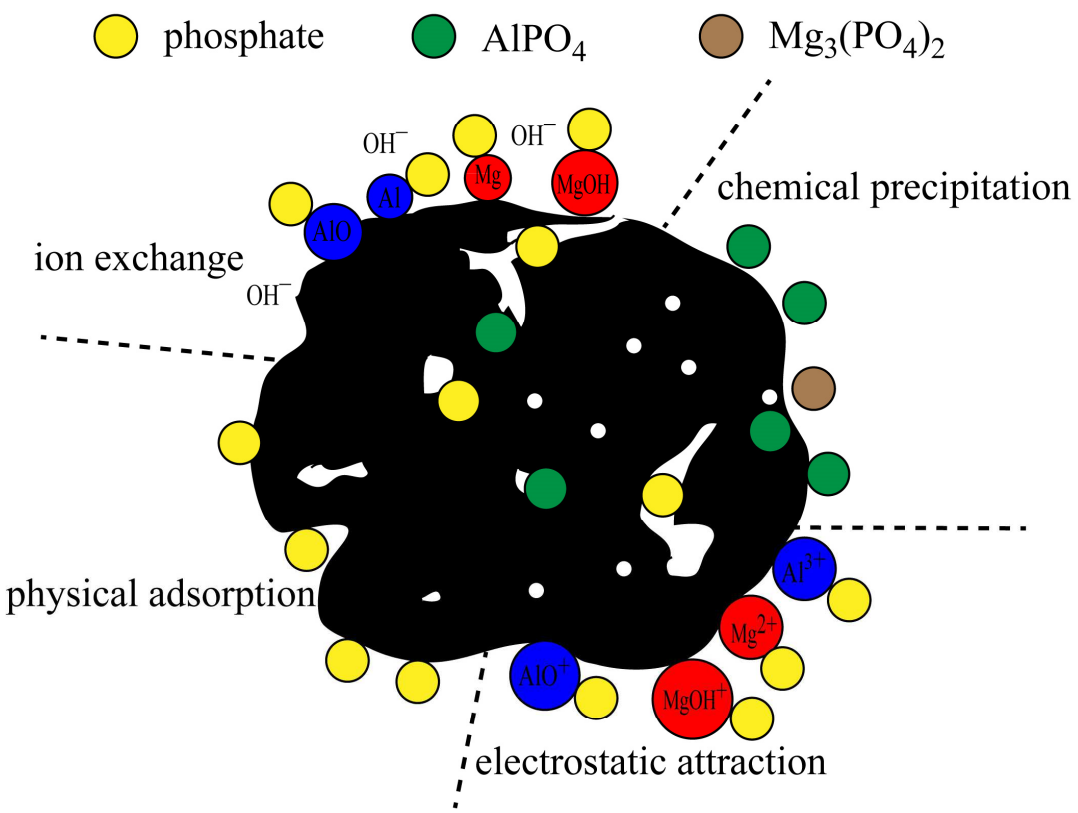
phosphate
AlPO4
Mg3(PO4)2
OH−
OH−
Mg
MgOH
Al
AlO
chemical precipitation
ion exchange
OH−
physical adsorption
Al3+
Mg2+
AlO+
MgOH+
electrostatic attraction

Fig. 5

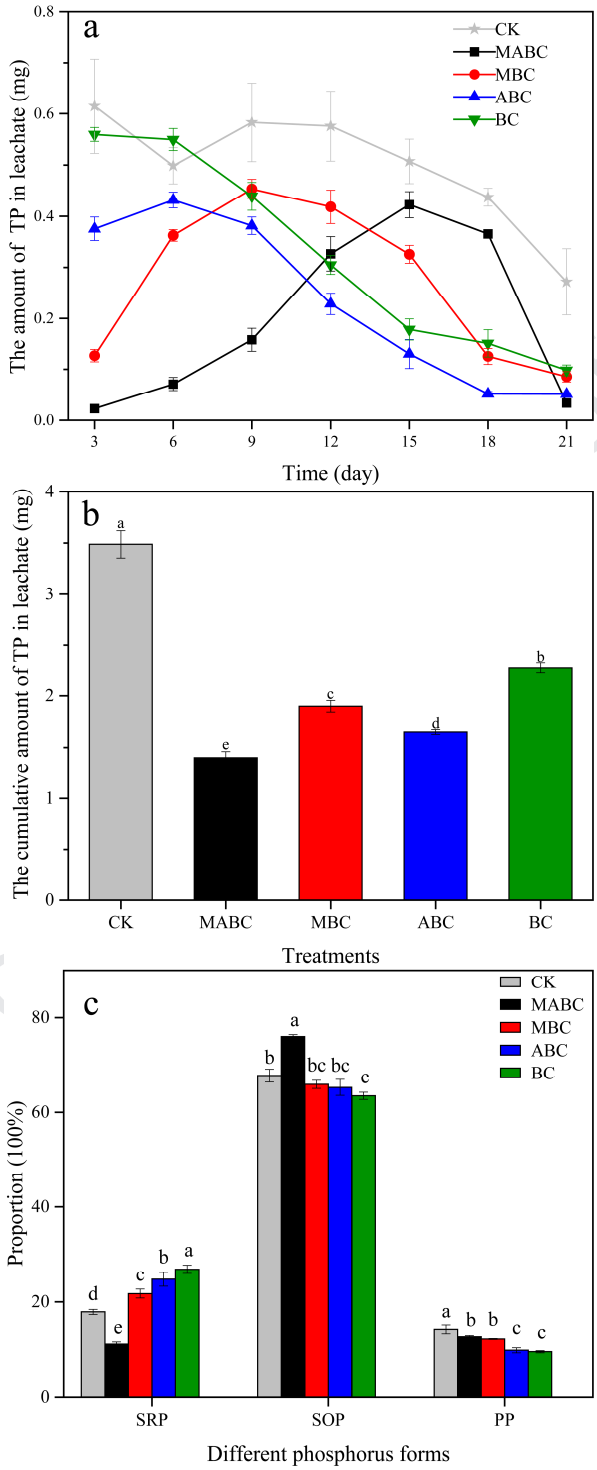
a
CK
MABC
MBC
ABC
BC
The amount of TP in leachate (mg)
Time (day)
b
The cumulative amount of TP in leachate (mg)
CK
MABC
MBC
ABC
BC
Treatments
c
Proportion (100%)
SRP
SOP
PP
Different phosphorus forms

Fig. 6

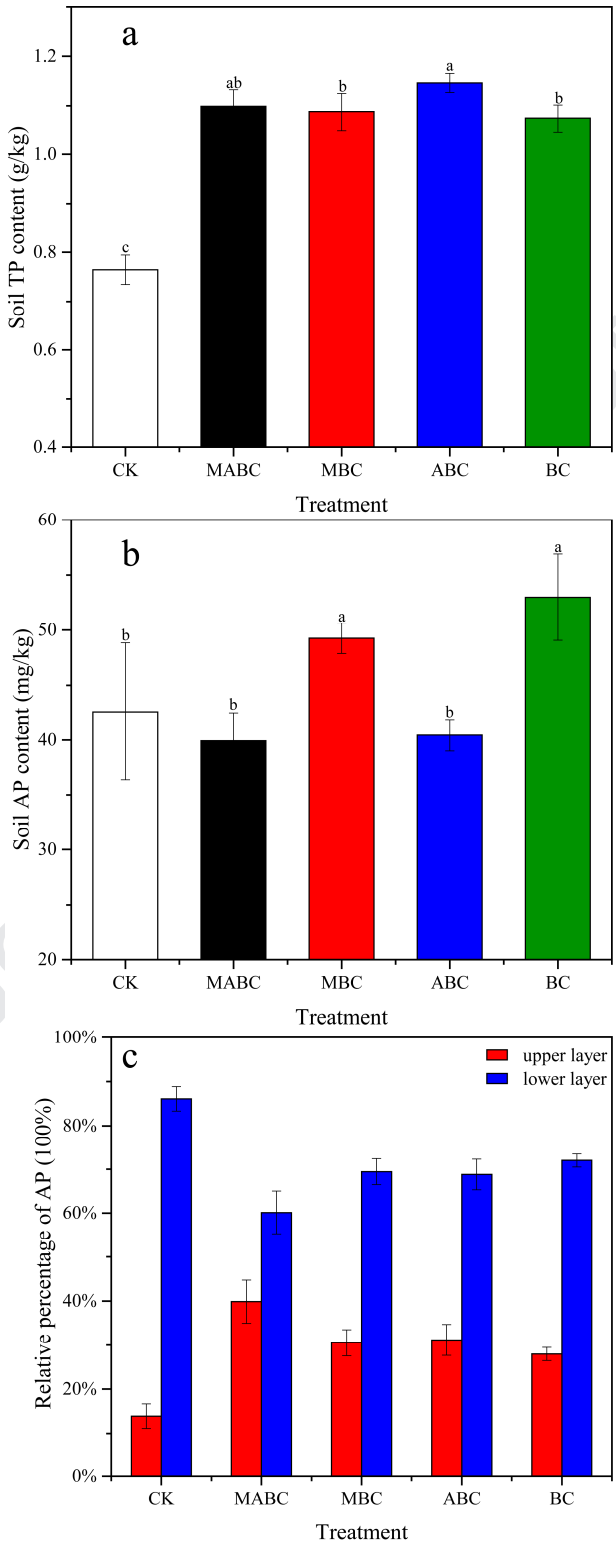
a
Soil TP content (g/kg)
1.2
1.0
0.8
0.6
0.4
c
ab
b
a
b
CK
MABC
MBC
ABC
BC
Treatment
b
Soil AP content (mg/kg)
60
50
40
30
20
b
b
a
b
a
CK
MABC
MBC
ABC
BC
Treatment
c
upper layer
lower layer
Relative percentage of AP (100%)
100%
80%
60%
40%
20%
0%
CK
MABC
MBC
ABC
BC
Treatment

Highlights

- Joint Mg- and Al-modified biochar (MABC) was prepared by co-precipitation.
- The surface of MABC found new crystal $MgAl_2O_4$.
- MABC exhibited excellent performance on phosphate adsorption.
- MABC had a potential for phosphate interception in soil.

Declaration of interests

■ The authors declare that they have no known competing financial interests or personal relationships that could have appeared to influence the work reported in this paper.

☐ The authors declare the following financial interests/personal relationships which may be considered as potential competing interests: